Experimental Evaluation of Robust Swing-Leg Placement Controls in Robotic Limb Testbeds

Alexander Schepelmann, Yin Zhong, Jessica Austin, Kathryn A. Geberth, and Hartmut Geyer

***Abstract*—Variable swing-leg placement is crucial for robust and stable locomotion. While appropriate leg placement is generated in humanoid robotics by tracking pre-planned swing motions, this approach is not suitable for controlling powered limbs like prostheses, which form only part of the human-robot locomotor system. In recent work, we proposed swing controls for a double pendulum leg model that predicts variable and robust leg placement in the presence of large gait disturbances. Here we evaluate the performance of these novel controls on robotic leg testbeds. In hardware experiments we find that the control achieves robust foot placement of anthropomorphic robotic limbs within a range of landing leg angles observed in human gait. We further observe that a version of this control that conforms with the constraints of neuromuscular dynamics generates a more human-like leg behavior at the cost of placement precision. The results suggest that the proposed controls transfer well to robotic limb systems; in particular, they may enable improved balance recovery in amputee locomotion with powered leg prostheses.**

***Index Terms*—Legged Locomotion, Swing-Leg, Humanoid, Prosthesis, Neuromuscular Control.**

I. Introduction

LEGGED animals and robots use foot placement to balance dynamically [1] [2] [3] [4] [5]. Successful foot placement first requires the identification of proper placement targets that stabilize locomotion, which can be obtained from simple point mass gait models in walking [6] [7] and running [8] [9]. Once identified, the second task is the control of the swing-leg into these targets, which is achieved in robotic applications in several ways. Humanoid systems use centralized control strategies that pre-plan and execute full-body trajectories using inverse dynamics and kinematics [10] [11]. These strategies have enabled robots to walk [12], climb stairs [13], and react to push disturbances [14] [15]. However, they are not suited for the control of robotic limbs such as prostheses, where the robot forms only part of the locomoting system.

While various control methods for robotic limbs exist, a significant number of control strategies in use today rely on the replay of joint patterns recorded from healthy human gait based on joint impedance [16] [17] [18], joint motion [19] [20], or a combination of the two [21]. These patterns implicitly encode appropriate foot placements for steady walking at various speeds and slopes, but do not enable foot-placement-based balance recovery after large disturbances such as trips, slips, and pushes. In response to this shortcoming, control extensions have been sought, for instance, to identify stumbles and generate predetermined recovery motions [22] [23], although no conclusive results have been presented about the effectiveness of these extensions.

In recent theoretical work, we proposed an alternative, heuristic swing-leg controller that takes advantage of the human leg's double pendulum dynamics to regulate foot placement [24]. In simulation, the controller places the foot point of the double pendulum into desired ground targets for a wide range of initial conditions and in the presence of substantial gait disturbances. In later work, this controller was reformulated to use virtual muscle actuators instead of ideal torque sources at the joints [25], and integrated into a muscle-reflex model of human locomotion [26]. Despite lacking central processing, the model walked over level and rough terrain, up stairs, and over obstacles. An initial evaluation of this muscle-reflex control on a transfemoral prosthesis suggested that this control can also generate qualitatively normal walking patterns in human-in-the-loop hardware [27]. While this performance suggests the proposed controls may enable robust foot placement in legged systems, it remains unclear how well they transfer from simulation to physical robot hardware and how the foot placement performance compares to that of widely used robotic limb controls.

In this paper, we transfer the proposed swing-leg controls to robotic hardware and evaluate their ability to regulate foot placement both when the leg's motion is undisturbed and when unknown obstacles are encountered during swing. For this transfer and evaluation, we extend our previous research on the implementation of the idealized swing-leg controller on robotic hardware [28] to include the neuromuscular control, to perform a comparison of both proposed controls against a benchmark impedance control in the presence of disturbances, and to extend this comparison in simulation to a generalized benchmark impedance control which incorporates a motion library to account for a range of target angles. Specifically, we compare the foot placement accuracy, swing duration, response behavior, and human-likeness of robotic leg testbeds under three swing-leg control strategies: the proposed idealized control, its neuromuscular reformulation, and a benchmark joint impedance control for powered prosthetic devices [29]. Work in this paper not only evaluates the proposed controls' relative performance to other controls in the context of benchmark impedance control, but also further explores the scalability of the proposed controls compared to existing methods used to regulate the motion of powered legged systems.

The authors are with the Robotics Institute, Carnegie Mellon University, Pittsburgh, PA, 15213 USA. E-mail: aschepel@alumni.cmu.edu, hgeyer@cmu.edu.

This work is supported by the Eunice Kennedy Shriver National Institute of Child Health & Human Development under award no. R01HD075492. A.S. is supported by the NSF GRF Program under grant 0946825.

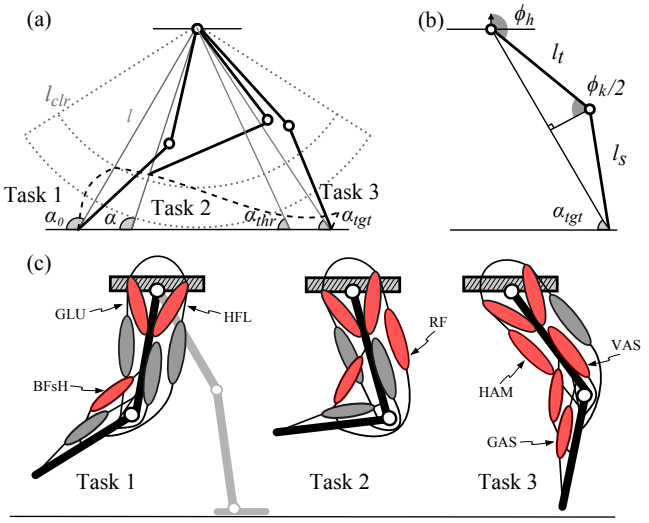

Fig. 1. Swing-leg control. (a) Task sequence. (b) Model geometry. (c) Active muscles during neuromuscular swing-leg control tasks. GLU: Gluteus. HFL: Hip Flexor. BFsH: Biceps Femoris Short Head. RF: Rectus Femoris. HAM: Hamstring. GAS: Gastrocnemius. VAS: Vastus.

In section II, we first summarize the proposed swing control both in its original form and its reformulation as a neuromuscular system. In section III, we then introduce the robotic testbeds and the hardware evaluation experiments, which show that the proposed controls achieve robust foot placements into a range of ground targets with a single set of high-level control gains. To further evaluate the proposed controls, we present high-fidelity simulations of the testbeds in section IV, and show that, compared to the implemented impedance control, the proposed swing-leg controls are highly scalable. Based on these findings, we finally discuss the potential of the identified limb controllers to help improve locomotion in legged robots and powered prostheses in section V.

II. Review of Proposed Control

A. Idealized swing-leg control

The swing-leg control proposed in [24] accomplishes foot placement into ground targets via combined hip and knee controls that are divided into three sequential tasks: leg flexion for ground clearance, leg advancement to a placement target, and leg extension until ground contact (Fig. 1a). Instead of tracking predefined joint trajectories to realize this sequence, the proposed control is based on heuristics. This approach is adopted for two reasons. First, tracking requires predefined motion libraries, which may not handle unexpected disturbances well. Second, a heuristic control approach can deliberately take advantage of favorable passive dynamics that reduce required motor torques.

The heuristics are developed using the leg length l and the leg angle α as the underlying coordinates of the swing leg double pendulum with $l = 2l_t \sin(\phi_k/2)$ and $\alpha = \phi_h - \phi_k/2$, respectively, assuming equal thigh and shank lengths (Fig. 1b). This coordinate transformation from the hip and knee angles, ϕ_h and ϕ_k, allows for a simple interpretation of the sequential control tasks. In addition, the proposed control is largely decoupled into distinct hip and knee controls, enabling its future use in modular powered prostheses. For the proposed controls, extension and flexion torques correspond to positive and negative torques, respectively.

1) Hip control: Hip control is active throughout swing. Its primary function is to drive the leg angle into a target angle α_{tgt} using

$$\tau_h = k_p^\alpha(\alpha_{tgt} - \alpha) - k_d^\alpha \dot{\alpha}, \tag{1}$$

where k_p^α and k_d^α are proportional and derivative gains. The target angle represents the ground target and is a free parameter. The hip control applies an additional torque τ_h^{iii} during late swing, which counters the effect of leg braking torque generated by the knee controller on the hip motion as $\tau_h^{iii} = -2\tau_k^{iii}$. This term is further explained in the following section.

2) Knee control: The knee control regulates the leg length l. It is separated into three sequential tasks by a finite state machine (Fig. 1a). In the first task, the goal is to flex the leg to a predefined ground clearance length l_{clr}. Instead of active regulation, however, passive double pendulum dynamics are exploited to achieve this goal. This leads to a control

$$\tau_k^i = \begin{cases} k^i \dot{\alpha} & \dot{\alpha} \leq 0 \\ 0 & \dot{\alpha} > 0 \end{cases}, \tag{2}$$

where active knee flexion is provided only if the leg moves forward ($\dot{\alpha} \leq 0$). The gain k^i determines flexion strength in proportion to the speed of forward motion. If $\dot{\alpha} > 0$, the knee is flexing passively and no action is needed to achieve l_{clr}.

Once the leg has flexed sufficiently ($l < l_{clr}$), the knee control switches to the second task of maintaining leg length with

$$\tau_k^{ii} = \begin{cases} -k^{ii}\dot{\phi}_k & \dot{\phi}_k \leq 0 \\ -k^{ii}\dot{\phi}_k(\alpha - \alpha_{tgt})(\dot{\phi}_k + \dot{\alpha}) & \dot{\phi}_k > 0 \;\&\; \dot{\phi}_k > -\dot{\alpha} \\ 0 & otherwise \end{cases}. \tag{3}$$

Knee flexion ($\dot{\phi}_k \leq 0$) is opposed with pure damping (derivative gain k^{ii}). Damping is also applied to slow down knee extension ($\dot{\phi}_k > 0$) but relaxed in proportion to how close the leg is to its target angle and how fast it approaches this target.

The knee control switches to the final task of braking and extending the leg once the leg angle passes a threshold $\alpha_{thr} = \alpha_{tgt} + \Delta\alpha_{thr}$. A stopping torque

$$\tau_k^{iii} = \begin{cases} -k^{stp}(\alpha_{thr} - \alpha)(1 - \frac{\dot{\alpha}}{\dot{\alpha}_{max}}) & \alpha < \alpha_{thr}, \dot{\alpha} < \dot{\alpha}_{max} \\ 0 & otherwise \end{cases} \tag{4}$$

is applied that is inspired by nonlinear contact models and acts like a virtual wall [30] [31]. The parameters k^{stp} and $\dot{\alpha}_{max}$ describe the stiffness and damping of this virtual wall interaction. Once the leg angular velocity has slowed to zero, $\dot{\alpha}$=0, a knee extension torque

$$\tau_k^{iii'} = \tau_k^{iii} + k^{ext}(l_0 - l) \tag{5}$$

is added to ensure the leg extends and seeks ground contact at the end of swing (proportional gain k^{ext}, $l_0 = l_t + l_s$).

B. Neuromuscular interpretation

The neuromuscular interpretation of the above control, originally presented in [25], embeds the swing-leg control (Eqs. 1-5) for an anthropomorphic leg model with simulated mono- and bi-articular muscle actuators. These muscle actuators can only pull and are activated by physiologically plausible reflex loops (Fig. 1c). We pursue this interpretation in addition to the idealized control implementation as the inclusion of muscle morphology and neural control limitations in the controller could lead to more human-like motion patterns, an outcome important to amputee locomotion. Specifically, the following virtual muscle groups are implemented in this neuromuscular controller: gluteus (GLU), hip flexor (HFL), biceps femoris short head (BFsH), rectus femoris (RF), hamstring (HAM), gastrocnemius (GAS), and vastus (VAS).

The muscles are modeled as Hill-type muscles with a non-linear relationship between their joint torque contribution, their neural stimulation, and the leg geometry, $\tau_j^m = f(\phi_h, \phi_k, S^m)$ (joint index j, muscle index m) [30]. Muscle stimulations are generated by reflex control loops and take the general form

$$S^m(t) = S_0^m + \sum_n G_n^m P_n^m(t - \Delta t_n^m), \tag{6}$$

where n is the index of the muscle contributing a reflex loop to the stimulation of muscle m, G_n^m is the reflex gain, P_n^m is the proprioceptive signal, and Δt_n^m is the reflex delay. Proprioceptive signals are either length L_n^m or velocity V_n^m of muscle n, and are modeled as

$$L_n^m = l_{ce}^n - l_{off}^n \text{ and } V_n^m = v_{ce}^n - v_{off}^n, \tag{7}$$

where l_{ce}^n and v_{ce}^n are the muscle's contractile element length and velocity, respectively, and l_{off}^n and v_{off}^n are offsets. In particular, the length and velocity signals of the bi-articular leg muscles HAM and RF can be used to interpret the leg angle and leg angular velocity (see Fig. 1 for muscle names and abbreviations), the length and velocity signals of the mono-articular knee muscles VAS and BFsH can be used to interpret knee angle and velocity, and the length and velocity offsets can be used to interpret threshold values.

1) Neuromuscular hip control: The hip control is interpreted in the neuromuscular model by mimicking the proportional term in Eq. 1 with stimulations of the hip extensor and flexor muscles (GLU and HFL),

$$S^{GLU}(t) = S_0^{GLU} + G_{HAM}^{GLU} L_{HAM}^{GLU}(t - \Delta t_{HAM}^{GLU}), \tag{8}$$
$$S^{HFL}(t) = S_0^{HFL} + G_{RF}^{HFL} L_{RF}^{HFL}(t - \Delta t_{RF}^{HFL}), \tag{9}$$

based on length reflexes from the bi-articular leg muscles (HAM and RF). As muscle behavior is automatically damped, the explicit damping term of Eq. 1 is neglected.

C. Swing-leg testbeds

1) Neuromuscular knee control: The first control task (Eq. 2) is realized by stimulating the mono-articular knee flexor BFsH with a reflex based on the velocity of RF,

$$S^{BFsH,i}(t) = G_{RF}^{BFsH} V_{RF}^{BFsH}(t - \Delta t_{RF}^{BFsH}), \tag{10}$$

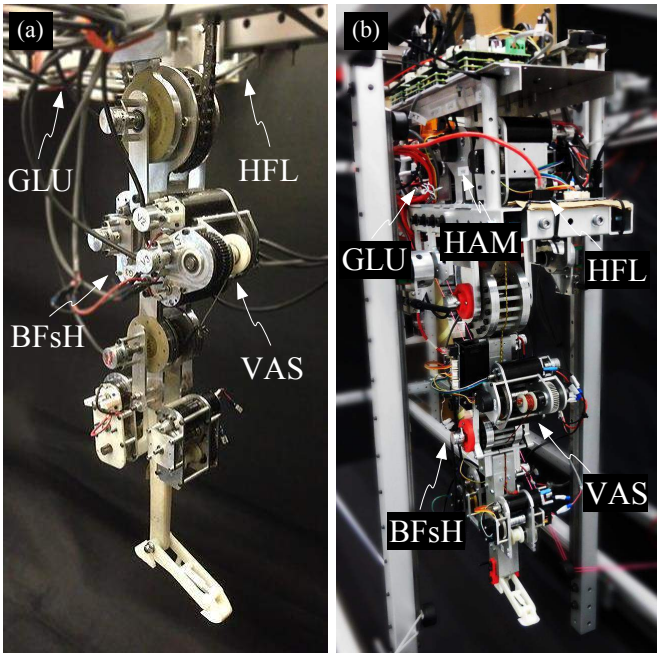

Fig. 2. Hardware testbeds RNL 2 (a) and 3 (b) for evaluating swing controls.

with $v_{off}^{RF} = 0$. For the second control task, knee flexion (first line in Eq. 3) is counteracted with the stimulation of RF based on a stretch velocity reflex from VAS,

$$S^{RF,ii}(t) = G_{VAS}^{RF} V_{VAS}^{RF}(t - \Delta t_{VAS}^{RF}), \tag{11}$$

and knee extension is resisted with the stimulation of BFsH based on its own velocity reflex,

$$S^{BFsH,ii}(t) = G_{BFsH}^{BFsH} V_{BFsH}^{BFsH}(t - \Delta t_{BFsH}^{BFsH}) M. \tag{12}$$

Here, M mimics the relaxation terms in Eq. 3 with additional reflexes based on the length of RF and the velocities of BFsH and RF,

$$M = L_{RF}^{BFsH}(t - \Delta t_{RF}^{BFsH}) \times [V_{BFsH}^{BFsH}(t - \Delta t_{BFsH}^{BFsH}) + V_{RF}^{BFsH}(t - \Delta t_{RF}^{BFsH})]. \tag{13}$$

The third control task (Eq. 4) is primarily realized with the bi-articular HAM, which is stimulated by its own length reflex,

$$S^{HAM,iii}(t) = G_{HAM}^{HAM} L_{HAM}^{HAM}(t - \Delta t_{HAM}^{HAM}). \tag{14}$$

If this stimulation surpasses a threshold S_{thr}, BFsH and GAS are additionally recruited to assist in braking with

$$S^{BFsH,iii}(t) = G_{HAM}^{BFsH}[S^{HAM,iii}(t) - S_{thr}], \tag{15}$$
$$\tag{16}$$

$$S^{GAS,iii}(t) = G_{HAM}^{GAS}[S^{HAM,iii}(t) - S_{thr}]. \tag{17}$$

Additionally, the mono-articular knee extensor VAS is stimulated by its own stretch reflex,

$$S^{VAS,iii}(t) = G_{VAS}^{VAS} L_{VAS}^{VAS}(t - \Delta t_{VAS}^{VAS}), \tag{18}$$

to embed Eq. 5 once the leg angular velocity has slowed to zero.

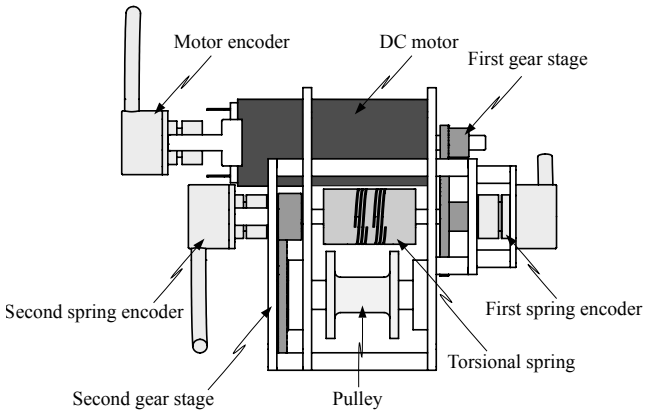

Fig. 3. Drivetrain schematic of RNL series elastic actuators.

TABLE I
SEA CAPABILITIES. THE SEAS MIMIC MAJOR LEG MUSCLES. THE MAXIMUM TORQUES AND SPEEDS ARE DYNAMICALLY SCALED ACCORDING TO [32].

	τ_j^{max} (Nm)	$\dot{\theta}_j^{max}$ (rpm)	n_{tot}	k_s (Nm/rad)
GLU	90	109	72	44.5
HFL	90	109	72	48.9
HAM	90	109	72	44.5
VAS	45	217	36	49.3
GAS	10	200	42.5	23.9

III. EXPERIMENTAL EVALUATION

The controls presented in the previous section achieve robust swing-leg placement in simulation [24] [25], but it is unclear how well they transfer to robotic hardware. Furthermore, it is unclear how the performance of the proposed controls compares to impedance control [29], the benchmark control method used to regulate robotic limb motions. The following sections present the "Robotic Neuromusuclar Leg" (RNL) locomotion testbeds and report on the experiments used to evaluate the performance of the proposed swing-leg controls in hardware.

RNL2 and RNL3 are legged robotic test platforms used to evaluate the proposed swing-leg controls on hardware (Fig. 2). The robots are dynamically scaled, antagonistically actuated robotic legs with translational joint compliance at the hip and knee. Their weight, size, and actuation requirements are based on dynamically scaled segment masses and lengths of a neuromechanical model of human locomotion [30], which is further described in [32].

The joints of the robots are antagonistically actuated by series elastic actuators (SEAs) that attach to the joints via cable-drives. Cable-driven SEAs mimic major muscle tendon units of the human model, which can go slack and enable truly passive swing-leg dynamics. Cable drives also enable the relocation of actuators away from joints, resulting in more human-like segment mass distributions. In total, RNL2 and RNL3 are actuated by four and five SEAs, respectively. The maximum joint torque τ_j^{max}, maximum joint speed $\dot{\theta}_j^{max}$, total gear ratio from rotor shaft to joint n_{tot}, and the spring stiffness k_s, of each SEA are summarized in table I. The RNL3 testbed is derived from the RNL2 platform. To retain dynamic similarity between the test platforms and human legs, bi-articular actuation, a key aspect of the neuromuscular control scheme, was implemented mechanically using an additional series elastic actuator that represents the hamstring. This required the robot's joints to be redesigned to accommodate a a bi-articular actuator cable that spans both the hip and knee joints. This is the key functional difference between the two platforms used to evaluate the proposed control schemes.

All SEAs follow the same drivetrain layout, using electric DC motors that are selected to meet the desired maximum joint torque and speed targets while remaining within the specified size and weight envelope (Fig. 3). The robots' GAS actuators use a single DC motor (Maxon Motor AG, RE30); all other actuators active during swing-leg control use two mechanically coupled DC motors for compactness (RE40). Torsional springs serve as the compliant elements of the SEAs and are located after the first gear stage. Off-the-shelf spring couplers are used as the SEAs' compliant elements (Ruland Manufacturing Co., GAS: FCMR19-5-5-A; all others: MWC25-6-6-SS).

Sensing and actuator control is implemented as a real-time 1kHz system using Simulink Realtime software (Mathworks, Inc.) and EtherCAT motor controllers (Advanced Motion Controls, DZEANTU-020B0808B, DZEANTU-040B0808B). Behavior control is also implemented in Simulink Realtime, operating at 1kHz for idealized swing-leg and impedance control and at 5kHz for neuromuscular control. SEA torque measurements in RNL2 are realized with two absolute rotary encoders (Renishaw PLC, RM22SC 13B) located on either side of the spring and are fed asynchronously to the target machine using a micrcontroller (Atmel Corporation, ATmega328-PU). SEA torque measurements in RNL3 are realized with two incremental encoders (US Digital, E2-5000-197-IE-D-D-B) located on either side of the spring and are fed to the target machine using a microcontroller which acts as an EtherCAT device (Atmel Corporation, ATxmega128a1) [33].

A. Behavior control implementation

Idealized swing-leg control and impedance control are implemented on RNL2 using its four antagonistic hip and knee actuators (Fig. 2a). These controls generate desired net joint torques, which are distributed to the corresponding SEA antagonists based on sign, with positive torques representing extension torques. The actuators track these desired torques with a velocity-based control scheme [34]. Details of the idealized swing-leg behavior control have been provided in section II-A (Eqs. 1-5). For the comparison with impedance control, the swing-leg portion of the control presented in [29] is used. In our implementation of this control, joint torques

$$\tau_j = k_1(\theta_{j,des} - \theta_j) - k_2\theta_j^3 - b\dot{\theta}_j \tag{19}$$

are commanded to the SEAs of RNL2 based on the measured position θ_j and velocity $\dot{\theta}_j$ of each joint j, where the parameters k_1, k_2 and b realize virtual spring-dampers that drive the hip and knee joints toward desired set-points $\theta_{j,des}$. The set points and the other parameters are provided by a two-state state machine, which transitions from the first to the second state when the knee velocity of RNL2 becomes larger than

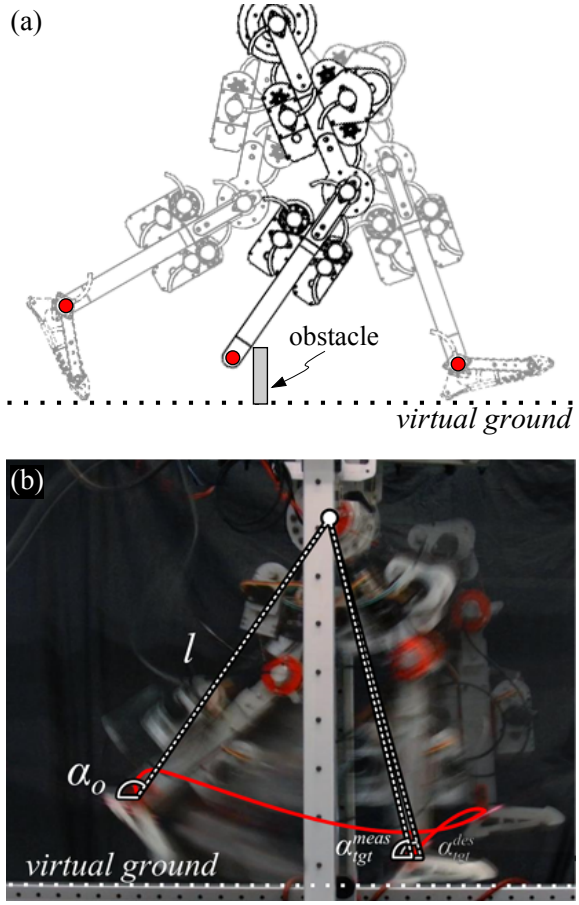

Fig. 4. Swing-leg motion experiments. (a) Experiment schematic keyframes: swing initialization, obstacle collision (disturbed experiments only), heel-strike. The geometry of a virtual foot constrained to be perpendicular to the shank is used to initialize the virtual ground location. Red: Ankle point. (b) RNL3 under neuromuscular swing-leg control during undisturbed experiment.

zero during the swing (transition from knee flexion to knee extension).

The neuromuscular swing-leg control is implemented on RNL3. RNL3 has five SEAs that represent the mono-articular hip muscles (GLU and HFL), the mono-articular knee muscles (VAS and BFsH), and the bi-articular hamstring (HAM) (Fig. 2b). The neuromuscular control (compare section II-B, Eqs. 9-18) generates a desired actuator torque for each of these muscle SEAs. In addition, the controller generates desired torques for the bi-articular rectus femoris (RF, eq. 11) and gastrocnemius (GAS, eq. 17), which RNL3 does not include in its current state of development. Instead, the effect of RF in the neuromuscular controller is simulated on RNL3 by adding its torque contributions simultaneously to the desired torques of the hip flexor and knee extensor muscle actuators (HFL and VAS, respectively), and the effect of GAS is simulated by adding its torque contributions to the desired torques of the knee flexor actuator (BFsH).

B. Experiment design

Two sets of experiments are used to evaluate the performance of the proposed controls and impedance control (Fig. 4). The first set tests the ability of the controllers to place the foot into desired ground targets during undisturbed swing. Each controller is tested for a range of target angles α_{tgt} from 65° to 90° with five trials per angle. The second set repeats the evaluation with an unexpected obstacle presented in early, mid, and late swing, respectively (Fig. 4a). The obstacle is a 600g wooden block on a set of rockers, approximating a tripping disturbance as the robot collides with the obstacle. In both sets of experiments, foot placement accuracy is assessed as the mean error between the desired and achieved leg angle at touchdown, and human-likeness of the control is assessed by comparing the resulting swing duration, response to unknown disturbances, and generated ankle point trajectory to the duration, obstacle response, and ankle trajectory of the human swing-leg in walking. Human reference data was extracted from motion capture (Vicon Motion Systems Limited, MX40) of a single subject walking at a self-selected speed of 1.3ms^{-1} (compare Fig. 6).

All experiments are initiated from a neutral, straight down configuration of RNL2 or RNL3. A feed-forward torque that is constant across all experiments then moves the leg into an initial pose of $\alpha_0 = 118^\circ$ with initial hip extension and knee flexion joint velocities mimicking the state of a human leg at swing initiation [24]. Once this pose is reached, the swing-leg controls initialize and regulate motion until the robot strikes a virtual ground, whose location is also initialized at this time. The location of the virtual ground is based on the geometry of a virtual dynamically scaled, anthropomorphic foot segment with a toe and heel, which is assumed to be locked in a perpendicular pose to the shank (Fig. 4). Across all experiments, the virtual ground is 5.25±0.2cm below the starting height of the ankle point after swing-leg control initialization.

For all swing-leg controllers, the control parameters are hand-tuned to achieve undisturbed swing motions to a target angle $\alpha_{tgt} = 70^\circ$, which corresponds to the landing angle observed in undisturbed, normal human walking [24]. RNL robots are assumed to have equal, nominal shank and thigh lengths of $l_t = l_s = 27$cm. Additional control parameters

TABLE II
IDEALIZED SWING-LEG CONTROL PARAMTERS.

parameter	value	parameter	value
k_p^α	38.7 Nm/rad	k^{ext}	260.9 N
k_d^α	0.2 Nms/rad	$\dot{\alpha}_{max}$	14.1 rad/s
k^i	2.8 Nms/rad	$\Delta\alpha_{thr}$	10°
k^{ii}	0.1 Nms/rad	l_{clr}	2 cm
k^{stp}	3.7 Nm/rad		

TABLE III
NEUROMUSCULAR CONTROL PARAMETERS. OTHER PARAMETERS ADAPTED FROM [30] AND [25] USING THE DYNAMIC SCALING LAWS IN [32].

parameter	value	parameter	value
G_{HAM}^{GLU}	0.14	G_{HAM}^{BFsH}	3.7
G_{RF}^{HFL}	2.3	G_{HAM}^{GAS}	2.6
G_{RF}^{BFsH}	0.54	G_{VAS}^{VAS}	0.77
V_{RF}^{BFsH}	0	G_{HAM}^{HAM}	1.9
G_{BFsH}^{BFsH}	1.0	S_{thr}	0.08

TABLE IV
IMPEDANCE CONTROL PARAMETERS.

parameter	value	parameter	value
$k_1^{hip,i}$	29.9 Nm/rad	$k_1^{hip,ii}$	15.9 Nm/rad
$k_2^{hip,i}$	18.6 Nm/rad^3	$k_2^{hip,ii}$	84.9 Nm/rad^3
$b^{hip,i}$	0 Nms/rad	$b^{hip,ii}$	0 Nms/rad
$\theta^{i}_{hip,des}$	170°	$\theta^{ii}_{hip,des}$	140°
$k_1^{knee,i}$	0.5 Nm/rad	$k_1^{knee,ii}$	71.8 Nm/rad
$k_2^{knee,i}$	4 Nm/rad^3	$k_2^{knee,ii}$	2 Nm/rad^3
$b^{knee,i}$	0 Nms/rad	$b^{knee,ii}$	0 Nms/rad
$\theta^{i}_{knee,des}$	120°	$\theta^{ii}_{knee,des}$	160°

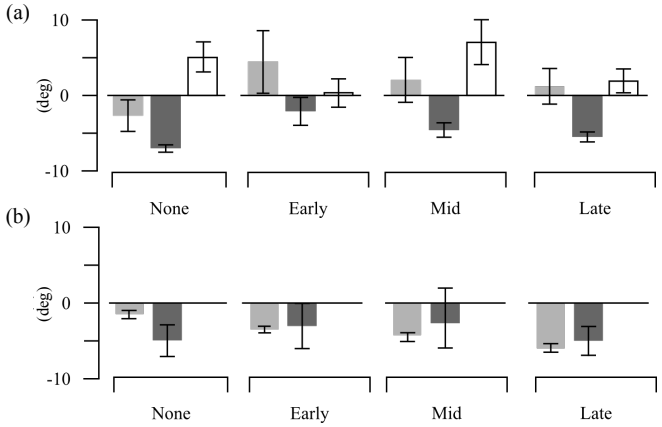

Fig. 5. Hardware foot placement error shown for the idealized control (light gray), neuromuscular control (dark gray), and impedance control (white). (a) Mean errors for the tuned-for target angle $\alpha_{tgt} = 70°$ achieved without obstacle encounter (none) and when an obstacle is present (early, mid, late). (b) Mean errors for the entire range of tested leg target angles $\alpha_{tgt} = 65°$ to $90°$. Bracketed lines show one standard deviation.

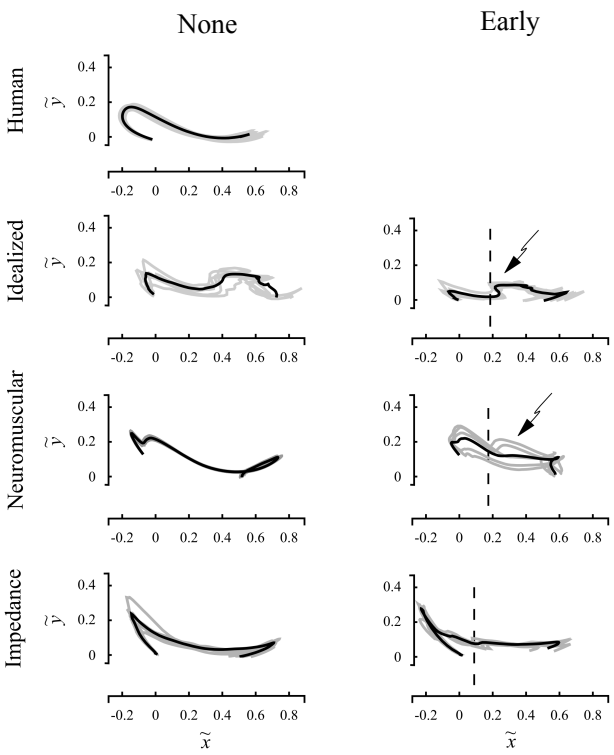

Fig. 6. Undisturbed (left column) and disturbed ankle trajectories with $\alpha_{tgt} = 70°$. Dashed line indicates obstacle location. Trajectories are normalized to subject and robot leg length, respectively (mean trajectories in black and individual traces in gray). The arrows highlight the visible disturbance responses to obstacle encounters in early swing. For the idealized control, this response consistently mimicked an elevation strategy. For the neuromuscular control, elevation was observed only in some cases.

are shown in tables II-IV. These parameters are used in all subsequent undisturbed and disturbed locomotion experiments.

C. Hardware results

Both idealized and neuromuscular swing-leg controllers can regulate foot placement into a range of desired ground targets in hardware (Fig. 5). The proposed controllers place feet into the tuned-for ground target of $\alpha_{tgt} = 70°$ with comparable accuracy to impedance control, both when the motion is undisturbed as well as when the robots encounter unknown disturbances in early, mid, and late swing (Fig. 5a). In addition, the variability of the foot placement achieved with the neuromuscular control in undisturbed swing (standard deviation, s.d., of $\pm 0.5°$) was similar to the foot placement variability observed in our subject data ($\alpha_{tgt} = 73.0 \pm 0.8°$, n=28), whereas the variability of both idealized swing-leg control and impedance control was larger (s.d. of $\pm 2.3°$ and $\pm 2.4°$, respectively). Due to impedance control's formulation as a set-point based torque controller that drives joints toward pre-specified angles (compare Eq. 19), it is not possible to use the same set of gains to place feet into a range of ground targets. Both the idealized and neuromuscular swing-leg control, on the other hand, enable foot placement into a range of ground targets by changing only the high-level α_{tgt} control parameter and retain foot placement accuracies comparable to the tuned-for "normal walking" condition (Fig. 5b).

Among the three tested swing-leg controls, the proposed neuromuscular control generates the most human-like swing leg behavior (Fig. 6). While trajectories generated by both the proposed neuromuscular control and impedance control are qualitatively similar to human trajectories for undisturbed swing, two-dimensional correlation (MathWorks MATLAB, *corr2*) between the human trajectory and each hardware trajectory of undisturbed swings shows that the neuromuscular control has the highest correlation (correlation coefficient R=0.89), followed by impedance control (R=0.81) and idealized control (R=0.71) (Fig. 6). Second, both the idealized and the neuromuscular control show responses to sudden swing-leg disturbances that can be qualitatively similar to human leg responses. Under idealized control, the robot performed an explicit foot point retraction and lifting in 88% of the experiments across the tested range of leg placement targets, akin to an elevation strategy observed in humans during trips that occur in early swing [35]. Under neuromuscular control, this early elevation strategy was observed in only 13% of the experiments, while the robot held the leg height after encountering an obstacle in 53% of experiments. Both controllers showed evidence of a lowering strategy for obstacle encounters in late swing (not shown in Fig. 6). In contrast, the

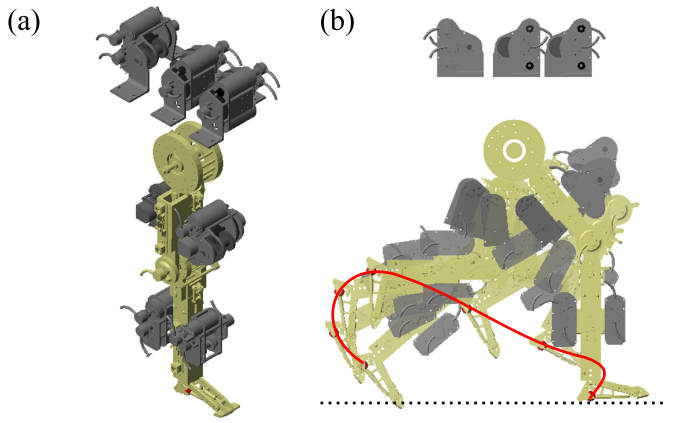

Fig. 7. RNL3 simulation. (a) Screenshot of RNL3 model. (b) Undisturbed trajectory experiment for $\alpha_{tgt} = 70^o$ with traced ankle point trajectory (red solid) and virtual ground (dotted) shown.

foot point trajectories for impedance control remained similar in all experimental conditions. This lack of a dynamic response stemmed from the fact that the impedance controller is based on joint angle set-points unaffected by obstacle encounters.

Finally, the swing duration of the neuromuscular control is closest to the swing duration of human walking, although all three controllers produce swing phases that last too long. Accounting for the dimensions of the robot testbeds, the dynamically scaled human swing duration should last between 180 ms and 360 ms for normal walking speeds [24]. With a duration of 415 ± 4ms neuromuscular control comes closest to this range, while the idealized control (519 ± 56ms) and impedance control (578 ± 32ms) last about 15% and 28% longer than the neuromuscular control. The difference in the swing duration between humans and the neuromuscular control could be related to motor saturation that we observed in the hip flexion actuator (HFL). The primary function of this actuator is to drive the leg towards the desired target, thus determining swing duration. However, further experiments with a stronger HFL would be necessary to test this hypothesis.

IV. Further Evaluation in Simulation

The hardware experiments in the previous section reveal that all three investigated controls can place the swing-leg foot with comparable accuracy when tuned for a specific target location (Fig. 5a); however, the experiments also show that the idealized and neuromuscular controls generalize to a wide range of ground targets using a single gain parameter set (Fig. 5b). To cover the same range of targets with similar performance using impedance control would require a motion library that contains explicit gain sets for various ground target locations across the desired foot placement range. These sets could serve as interpolation nodes to calculate appropriate impedance control gains for foot placement targets across the foot placement range. However, it is unclear how many explicit gain sets would be required across this range to achieve similar performance to the proposed controls. Due to the *in-situ* tuning process used to generate hardware gain sets, it is impractical to investigate this question on the testbeds directly. As such, we developed high-fidelity simulations of the robots, whose control parameters could be tuned via optimization. These simulations are used in the following section to investigate how extensive an impedance control motion library must be in order to achieve similar performance to the proposed controls over the foot placement range.

A. Simulated testbeds

The simulations of the RNL2 and RNL3 testbeds are developed in Simulink Simscape Multibody (Mathworks, Inc.) (Fig. 7). Besides replicating the behavior and motor controls used in the hardware experiments, the simulations model the electro-mechanics of the testbeds. Motor electrical dynamics are modeled as

$$V - iR - L\frac{di}{dt} - k_{EMF}\dot{\theta}_m = 0, \tag{20}$$

where V, i, R, L, k_{EMF}, and $\dot{\theta}_m$ are the motor voltage, current, resistance, inductance, back-EMF constant, and motor velocity [36]. A $\pm$48V saturation simulates voltage limits of the robots' motor controllers and voltage commands are generated with a PID loop operating on the difference between desired and measured motor velocity. The drivetrain stages (Fig. 3) are modeled as separate physical, interacting bodies, with the rotational inertias of each stage estimated from CAD models. Coulomb friction τ_f^c is applied to every bearing stage, whose coefficients are calculated from linear regression of experimental characterization data using $\tau_f^c = \mu_i sgn(\dot{\theta}_i)$, where μ_i is the offset of Coulomb friction at each drivetrain stage i with a velocity $\dot{\theta}_i$. Similarly, viscous friction is modeled for the robots' hip and knee joints with friction coefficients determined experimentally. The torsional stiffness values of the SEA springs are calculated from testbed experiments using analog compression load cells (FC22, 100lbf: Measurement Specialties) (Tab. I). The robots' cable drives, which connect SEA drivetrain outputs to the joints, are modeled as unidirectional series spring-dampers with a stiffness of 10kN/m and a damping constant of 500Ns/m.

B. Simulation experiments and results

We use the testbed simulations to study the effect of the motion library size on the placement accuracy for ground targets α_{tgt} ranging from 60^o to 90^o. First, we define three libraries differentiated by the number of nodes (target angles) for which impedance control is tuned: 3 nodes (70^o and the boundaries 60^o and 90^o), 4 nodes (60^o to 90^o in 10^o increments), and 7 nodes (60^o to 90^o in 5^o increments). Second, we tune the parameters of the impedance controller (Eq. 19) for each node with optimization (CMA-ES, [37]). The cost function used to tune the parameters is

$$J(\chi_n) = \sum_{i=1}^{4}(\alpha_{tgt}^i - \alpha_{td}^i)^2, \tag{21}$$

where χ is the vector of tuned parameters corresponding to node n, i is the index for the specific swing-leg case type encountered in hardware experiments (undisturbed swing, early-, mid-, and late-disturbance) that are described in Sec. III-B,

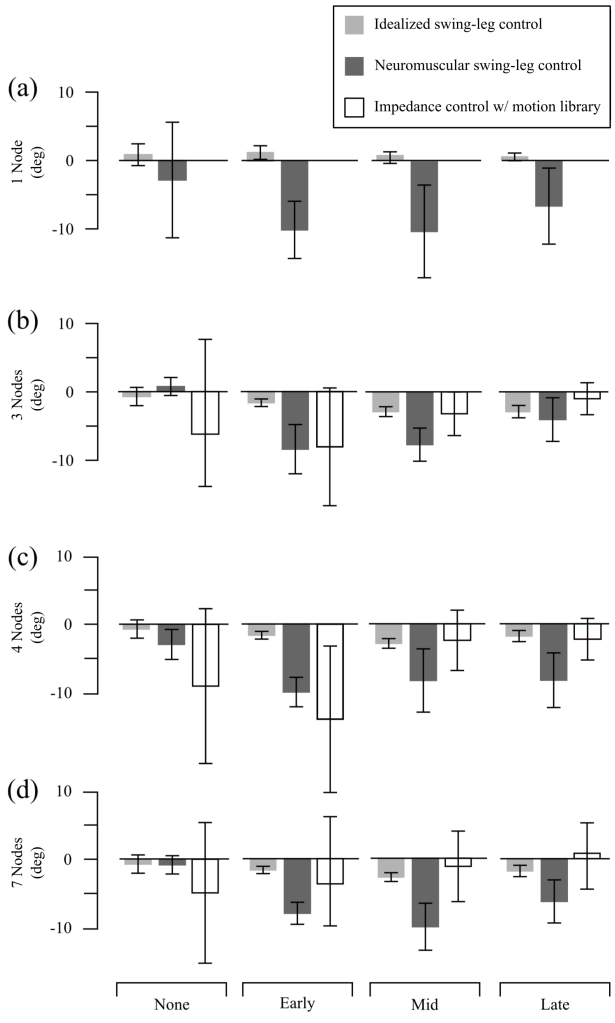

Fig. 8. Simulation foot placement errors of the proposed controls and impedance control with a motion library for an α_{tgt} range from 60^o to 90^o. Idealized swing-leg and impedance control simulation performed with the RNL2 model. Neuromuscular swing-leg control performed with the RNL3 model.

α_{tgt} is the desired foot placement target expressed as a touchdown angle, and α_{td} is the measured angle at touchdown. Finally, we evaluate the placement accuracy of the impedance control with motion libraries by simulating the hardware experiments over the range from 60^o to 90^o in 1^o increments. For inter-node target angles not stored in the libraries, the control draws from spline-interpolated parameters.

For a direct comparison between impedance control and the proposed controls, we follow a similar procedure with the idealized and neuromuscular controls. Instead of generating a motion library, however, we simultaneously optimize a single set of control parameters over all the experimental conditions used for tuning the corresponding library of impedance control. For instance, to compare to the impedance controller with a 3 node library, we tune the control parameters of the idealized and neuromuscular controls by minimizing the total placement error over 12 tuning experiments (four disturbance trials per target angle) to generate one set of control parameters. Thus, as in the hardware experiments (Sec. III-C), the idealized and neuromuscular controls each only have a single set of parameters to execute foot placements into the entire range of target angles.

Figure 8 summarizes the results of the comparison for leg placements throughout the entire range of target angles. Impedance control achieves a performance comparable to idealized and neuromuscular control for the disturbed conditions already with a 3 node library; but although the mean foot placement error decreases with an increase in size in the motion library, even at 7 tuning nodes, impedance control cannot match the performance of the proposed controls for undisturbed swing. In contrast, the foot placement errors for the idealized and neuromuscular controls remain about the same independent of the size of the tuning set, suggesting that a small set could suffice in practical applications. Indeed, tuning the proposed controls for a single locomotion condition that corresponds to nominal, undisturbed walking, enabled the testbeds to accurately place feet into ground targets over the tested range. In addition, substantially smaller standard deviations for the errors in undisturbed swings and in swings with early disturbance indicate that the placement performance of the proposed controls is less sensitive than that of impedance control.

V. Discussion

We investigated the performance of a novel swing-leg control in robotic leg testbeds. In hardware experiments on undisturbed swings and swings with unexpected obstacle encounters, we found that this control leads to robust foot placement of anthropomorphic robotic legs within a range of landing leg angles observed in human gait (Fig. 5). Impedance control, the benchmark alternative, achieved a similar placement performance at tuned-for targets, but requires a motion library to accommodate target ranges. In simulations of the robotic leg testbeds, we found that such a library-based impedance control can match the performance of the proposed controls only for disturbed swing motions (Fig. 8). The results suggest the proposed control as a candidate control for powered leg prostheses that need to react to unexpected tripping disturbances and to adapt foot placement to help amputees recover balance in locomotion.

The proposed controls likely outperform impedance control because the former considers the global pose of the leg, and because they were designed around the coupled, passive dynamics of a segmented leg. In impedance control, joint torque is generated based only on the motion of the local joint [17]. As a result, impedance control resembles a local and decoupled approximate solution about nominal swing trajectories that is sensitive to changes in the set point, in this case the target angle, despite the addition of a motion library (first column in Fig. 8). In contrast, the proposed controls consider both the global information about the leg and the inertial coupling effects across joints. The controls are formulated around the global coordinates of the leg angle and leg length (α, l), and the nonlinear feedback terms for the knee joint controls take advantage of inertial effects generated by the hip

motion (for instance, Eqs. 2–4); thus, the controllers become less dependent on the actual trajectory, achieving better foot placement accuracy with fewer control parameters for the investigated range of target angles. Note, however, that in the neuromuscular reformulation, the placement performance after recovery from disturbances does not seem to benefit from this advantage (columns two to four, Fig. 8). It remains an open question whether the proposed control strategy can improve over the placement accuracy of other, more centralized swing-leg control strategies, for instance those used in humanoid robotics [10] [11].

Besides foot placement accuracy, a second advantage of the proposed control is that it requires comparably few parameters to be tuned. With the growing complexity of powered prostheses, tuning their controllers is becoming an ever increasing challenge for clinical practice. Several alternative control and tuning methods have been proposed to reduce the number of parameters in stance [38] [39] [40]. The proposed controls achieve a similar reduction for the number of parameters to be tuned in swing (6 and 10 for the neuromuscular reformulation) while adding behavior versatility and robustness. Impedance control, on the other hand, already requires 16 parameters without a motion library (4 parameters in Eq. 19 times two phases for each joint), and would need considerably more with a motion library. Tuning-free swing-leg controls have also been recently proposed, but are kinematic in nature, enforcing motion patterns for undisturbed walking using virtual constraints [41] and minimum jerk trajectories [42]. While these controls enable users to dynamically walk at various speeds, they require an *a priori* notion of what the swing-leg motion will look like throughout the swing-phase, and their ability to walk robustly in the presence of significant motion disturbances has not been tested. As such, how the performance of these controls compare to those presented in this paper are unclear.

Whether a neuromuscular reformulation is preferable remains an open question as well. In our experiments, this control showed less placement accuracy while at the same time requiring more parameters than the idealized version of the proposed control. However, conforming with known properties of human motor control including muscle actuation dynamics and neural transmission delays, the neuromuscular reformulation produced the most human-like swing behavior among the investigated control strategies (Fig. 6). In applications like prosthetics, where cosmesis is a concern, trading off accuracy and parameter convenience against human-likeness may be preferable, although clarifying the effect of this trade-off on amputee gait will require experiments with amputee subjects wearing an actual prostheses.

We are currently working towards such an experimental evaluation on active prostheses in amputee gait. In preliminary tests with one non-amputee user wearing a powered leg-prosthesis prototype, we have found that the proposed control reproduces normal walking patterns and effectively responds to disturbances in early and late swing [27]. Although more research will be needed to improve the control implementation and to determine how well these results transfer to amputee gait, they highlight the potential of the proposed and other controls that consider global leg information for improving balance recovery, which despite the advances in prosthetic control and technology [43], remains one of the main concerns for transfemoral amputees [44].

ACKNOWLEDGMENT

The authors would like to thank L. Hayhurst and J. Dillinger for help with robot fabrication, T. Xu for help with sensor design, and R. Desai for help with early experiments.

REFERENCES

[1] M. Raibert, *Legged Robots that Balance*. MIT Press, 1986.
[2] M. S. Redfern and T. Schumann, "A model of foot placement during gait," *J. Biomech.*, vol. 27, no. 11, pp. 1339–1346, 1994.
[3] T. de Boer, "Foot placement in robotic bipedal locomotion," *Ph.D. Thesis, Technische Universiteit Delft*, 2012.
[4] M. Posa, T. Koolen, and R. Tedrake, "Balancing and step recovery capturability via sums-of-squares optimization," *Proc. RSS*, vol. 13, no. 1, 2017.
[5] Q. Nguyen, A. Agrawal, X. Da, W. Martin, H. Geyer, J. Grizzle, and K. Sreenath, "Dynamic walking on randomly-varying discrete terrain with one-step preview," *Proc. RSS*, vol. 13, no. 1, 2017.
[6] S. Kajita and K. Tani, "Study of dynamic biped locomotion on rugged terrain - derivation and application of the linear inverted pendulum mode," *Proc. IEEE ICRA*, pp. 1405–1411, 1991.
[7] M. A. Townsend, "Biped gait stabilization via foot placement," *J. Biomech.*, vol. 18, no. 1, pp. 21–38, 1985.
[8] R. Blickhan, "The spring-mass model for running and hopping," *J. Biomech.*, vol. 22, no. 11-12, pp. 1217–1227, 1989.
[9] A. Seyfarth, H. Geyer, and H. M. Herr, "Swing-leg retraction: A simple model for stable running," *J. Exp. Biol.*, vol. 206, no. 15, pp. 2547–2555, 2003.
[10] M. Fallon, S. Kuindersma, M. Antone, T. Schneider, H. D., C. P. D'Arpino, R. Deits, M. DiCicco, D. Fourie, T. Koolen, P. Marion, M. Posa, A. Valenzuela, K. T. Yu, J. Shah, K. Iagnemma, R. Tedrake, and S. Teller, "An architecture for online affordance-based perception and whole-body planning," *Journal of Field Robotics*, vol. 32, no. 2, pp. 229–254, 2015.
[11] S. Feng, E. Whitman, X. Xinjilefu, and C. G. Atkeson, "Optimization based full body control for the ATLAS robot," *Proc. IEEE-RAS Humanoid Robots*, pp. 120–127, 2014.
[12] S. Kajita, T. Nagasaki, K. Kaneko, and H. Hirukawa, "ZMP-based biped running control," *IEEE Rob. and Aut. Mag.*, vol. 14, no. 2, pp. 63–72, 2007.
[13] S. Kajita, F. Kanehiro, K. Kaneko, K. Fujiwara, K. Harada, K. Yokoi, and H. Hirukawa, "Biped walking pattern generation by using preview control of zero-moment point," *Proc. IEEE ICRA*, pp. 1620–1626, 2003.
[14] M. Spenko, K. Iagnemma, and S. Buerger, Eds., *J. Field Rob. Special Issue: The DARPA Robotics Challenge Finals*, vol. 34, no. 2, 2017.
[15] J. Urata, K. Nshiwaki, Y. Nakanishi, K. Okada, S. Kagami, and M. Inaba, "Online walking pattern generation for push recovery and minimum delay to commanded change of direction and speed," *Proc. IEEE/RSJ IROS*, pp. 3411–3416, 2012.
[16] J. A. Blaya and H. M. Herr, "Adaptive control of a variable-impedance ankle-foot orthosis to assist drop-foot gait," *IEEE Trans. N. Syst. Rehab. Eng.*, vol. 12, no. 1, pp. 968–977, 2012.
[17] F. Sup, H. A. Varol, and M. Goldfarb, "Upslope walking with a powered knee and ankle prosthesis: Initial results with an amputee subject," *IEEE Trans. N. Syst. Rehab. Eng.*, vol. 19, no. 1, pp. 71–78, 2011.
[18] A. M. Simon, K. A. Ingraham, N. P. Fey, S. B. Finucane, R. D. Lipschutz, A. J. Young, and H. L. J., "Configuring a powered knee and ankle prosthesis for transfemoral amputees within five specific ambulation modes," *PLoS One*, vol. 9, no. 6, p. e99387, 2014.
[19] J. Hitt, A. M. Oymagil, T. Sugar, K. Hollander, B. A., and J. Fleeger, "Dynamically controlled ankle-foot orthosis (DCO) with regenerative kinematics: Incrementally attaining user portability," *Proc. IEEE ICRA*, pp. 1541–1546, 2007.
[20] P. D. Neuhaus, J. H. Noorden, T. J. Craig, T. Torres, J. Kirschbaum, and J. E. Pratt, "Design and evaluation of Mina: A robotic orthosis for paraplegics," *Proc. IEEE ICORR*, pp. 1–8, 2011.
[21] S. K. Au, H. Herr, J. Weber, and E. Martinez-Villalpando, "Powered ankle-foot prosthesis for the improvement of amputee ambulation," *Proc. IEEE EMBS*, pp. 3020–3026, 2007.

[22] B. E. Lawson, "Control methodologies for powered prosthetic interventions in unilateral and bilateral transfemoral amputees," Ph.D. dissertation, Vanderbilt University, 2014.
[23] B. E. Lawson, H. A. Varol, F. Sup, and M. Goldfarb, "Stumble detection and classification for an intelligent transfemoral prosthesis," *Proc. IEEE EMBC*, pp. 511–514, 2010.
[24] R. Desai and H. Geyer, "Robust swing leg placement under large disturbances," *Proc. IEEE ROBIO*, pp. 265–270, 2012.
[25] ——, "Muscle-reflex control of robust swing leg placement," *Proc. IEEE ICRA*, pp. 2169–2174, 2013.
[26] S. Song and H. Geyer, "A neural circuitry that emphasizes spinal feedback generates diverse behaviours of human locomotion," *J. Physiol.*, vol. 593, no. 16, pp. 3493–3511, 2015.
[27] N. Thatte and H. Geyer, "Toward balance recovery with leg prostheses using neuromuscular model control," *IEEE Trans. Biomed. Eng.*, pp. 904–913, 2016.
[28] A. Schepelmann, J. Austin, and H. Geyer, "Evaluation of decentralized reactive swing-leg control on a powered robotic leg," *Proc. IEEE/RSJ IROS*, pp. 381–386, 2015.
[29] F. Sup, A. Bohara, and M. Goldfarb, "Design and control of a powered transfemoral prosthesis," *International Journal of Robotics Research (IJRR)*, vol. 27, no. 2, pp. 263–273, 2008.
[30] H. Geyer and H. M. Herr, "A muscle-reflex model that encodes principles of legged mechanics produces human walking dynamics and muscle activities," *IEEE Trans. N. Sys. Rehab. Eng.*, vol. 18, no. 3, pp. 263–273, 2010.
[31] K. Hunt and F. Crossley, "Coefficient of restitution interpreted as damping in vibroimpact," *J. App. Mech.*, vol. 42, no. 2, pp. 440–445, 1974.
[32] A. Schepelmann, M. D. Taylor, and H. Geyer, "Development of a testbed for robotic neuromuscular controllers," *Proceedings RSS*, vol. 8, no. 1, pp. 385–392, 2012.
[33] O. S. U. D. R. Laboratory, "Medulla: A simple embedded EtherCAT slave device using a xMega microcontroller," 2012. [Online]. Available: https://code.google.com/p/medulla/
[34] M. D. Taylor, "A compact series elastic actuator for bipedal robots with human-like dynamic performance," *M.S. Thesis, Carnegie Mellon University*, 2011.
[35] J. J. Eng, D. A. Winter, and A. E. Patla, "Strategies for recovery from a trip in early and late swing during human walking," *Experiemental Brain Research*, vol. 102, no. 2, pp. 339–349, 1994.
[36] B. Siciliano, L. Sciavicco, L. Villani, and G. Oriolo, *Robotics: Modelling, Planning and Control*. Springer, 2009.
[37] N. Hansen, "CMA-ES MATLAB implementation (version 3.61) [Computer program]," 2013. [Online]. Available: https://www.lri.fr/%7Ehansen/cmaes.m
[38] A. M. Simon, N. P. Fey, S. B. Finucane, R. D. Lipschutz, and L. J. Hargrove, "Strategies to reduce the configuration time for a powered knee and ankle prosthesis across multiple ambulation modes," *IEEE International Conference on Rehabilitation Robotics*, pp. 1–6, 2013.
[39] R. D. Gregg, T. Lenzi, L. J. Hargrove, and J. W. Sensinger, "Virtual constraint control of a powered prosthetic leg: From simulation to experiments with transfemoral amputees," *IEEE Transactions on Robotics*, vol. 30, no. 6, pp. 1455–1471, 2014.
[40] H. Huang, D. Crouch, M. Liu, G. S. Sawicki, and D. Wang, "A cyber expert system for auto-tuning powered prosthesis impedance control parameters," *Annals of Biomedical Engineering*, vol. 44, no. 5, pp. 1613–1624, 2016.
[41] D. Quintero, D. J. Villarreal, and R. D. Gregg, "Preliminary experiments with a unified controller for a powered knee-ankle prosthetic leg across walking speeds," *Proc. IEEE/RSJ IROS*, pp. 5427–5433, 2016.
[42] T. Lenzi, L. Hargrove, and J. Sensinger, "Speed-adaptation mechanism: Robotic prostheses can actively regulate joint torque," *IEEE Rob. Autom. Mag.*, vol. 21, no. 4, pp. 94–107, 2016.
[43] M. R. Tucker, J. Olivier, A. Pagel, H. Bleuler, M. Bouri, O. Lambercy, J. del R. Millan, R. Riener, H. Vallery, and R. Gassert, "Control strategies for active lower extremity prosthetics and orthotics: a review," *Journal of NeuroEngineering and Rehabilitation*, vol. 12, no. 1, pp. 1–29, 2015.
[44] K. Hagberg and R. Branemark, "Consequences of non-vascular transfemoral amputation: A survey of quality of life, and prosthetic use and problems," *Prosthetics and Orthotics International*, vol. 25, pp. 186–194, 2001.